Multiphoton endoscopy

Juergen C. Jung

Bell Laboratories, Lucent Technologies, 600 Mountain Avenue, Murray Hill, New Jersey 07974, and Department of Pharmacology, Oxford University, Mansfield Road, Oxford OX1 3QT, UK

Mark J. Schnitzer

Bell Laboratories, Lucent Technologies, 600 Mountain Avenue, Murray Hill, New Jersey 07974

Received December 4, 2002

Despite widespread use of multiphoton fluorescence microscopy, development of endoscopes for nonlinear optical imaging has been stymied by the degradation of ultrashort excitation pulses that occurs within optical fiber as a result of the combined effects of group-velocity dispersion and self-phase modulation. We introduce microendoscopes (350−1000 μm in diameter) based on gradient-index microlenses that effectively eliminate self-phase modulation within the endoscope. Laser-scanning multiphoton fluorescence endoscopy exhibits micrometer-scale resolution. We used multiphoton endoscopes to image fluorescently labeled neurons and dendrites. © 2003 Optical Society of America

OCIS codes: 170.2150, 170.2520, 170.5810, 170.3880, 170.1790.

Multiphoton fluorescence imaging offers a key advantage for imaging within strongly scattering biological media: depth sectioning without use of a confocal pinhole for excluding out-of-focus fluorescence.[1] Sectioning arises because the N-photon excitation rate per fluorophore decays sharply with axial distance from the focal plane.[2] Since fluorescence originates from a limited excitation volume, scattered fluorescence signals need not be wastefully discarded by a pinhole in the detection optics. Other advantages over conventional confocal fluorescence imaging include reduced out-of-focal-plane photobleaching and photodamage and reduced scattering of incident light by use of longer-wavelength excitation. These combined benefits often make multiphoton microscopy superior to confocal microscopy for imaging at focal depths hundreds of micrometers below the surface of highly scattering tissue slices or within live animals.[1]

Nonetheless, confocal imaging has been adapted to the realm of endoscopy,[3–8] whereas until now multiphoton imaging has not been. Compact[9] and miniature[10] multiphoton microscopes that use single-mode fiber (SMF) for excitation light delivery have been incapable of delivering femtosecond excitation pulses at nanojoule energies for imaging deep within highly scattering biological tissue.[1] We report the design, construction, and application of multiphoton fluorescence endoscopes (350–1000-μm diameter, Fig. 1a) that are based on gradient-index (GRIN) lenses and that can deliver femtosecond pulses up to nanojoule energies.

Why is it that confocal endoscope designs do not extend to multiphoton imaging? Over SMF lengths as short as 1–10 cm, femtosecond pulses degrade as a result of the combined effects of group-velocity dispersion (GVD) and self-phase modulation (SPM).[9–13] GVD in SMF can be precompensated for by use of gratings to provide negative chirping,[10–13] albeit at power loss, but SPM is a nonlinear optical effect that causes negatively chirped pulses to undergo spectral narrowing. Thus, prechirped ~100-fs pulses of 0.1–1 nJ broaden to 0.2–1 ps after ~1 cm of travel in SMF.[11–13]

Increasing laser power to boost fluorescence can partially compensate for this effect, but increased pulse energy, E, leads to further spectral changes. Two-photon fluorescence excited by prechirped pulses delivered through SMF increases only as $E^{1.25}$ (Ref. 14) rather than as E^2. A subquadratic increase in two-photon fluorescence occurs for E above ~0.1 nJ (8-mW average power at 80-MHz repetition rates[13]) and provides a convenient diagnostic for SPM effects. Our laser-scanning endoscopes avoid high intensities and resultant SPM that arise when ultrashort pulses are confined to the 5–10-μm mode field diameter of SMF.

We developed epifluorescence microendoscope probes that are 0.9–2.6 cm in length and 350–1000 μm in diameter and that are based on GRIN microlenses (Fig. 1). When used as stand-alone rigid endoscopes,

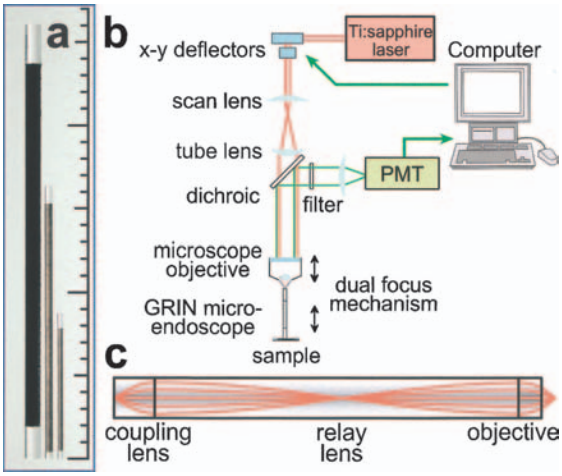

Fig. 1. a, Photograph of three multiphoton endoscopes, of 1.0-, 0.5-, and 0.35-mm diameter, oriented with the coupling lens at the top of the figure. A minor tick on the scale equals 1.0 mm. b, Optical layout used for the endoscopic measurements of Figs. 2 and 3. The focal plane in the sample may be adjusted by movement of either the endoscope itself or the microscope objective that couples the excitation beam. PMT, photomultiplier tube. Custom software controlled a pair of galvanometers (Cambridge Technologies) for $x-y$ scanning. c, Optical schematic of the excitation beam in the endoscope GRIN triplet. Red lines are normal to the local wave fronts.

0146-9592/03/110902-03$15.00/0

as shown here, our microendoscopes provide the ability to make focal adjustments by moving intermediate optics on the side of the relay that is external to the sample (Fig. 1b). Our probes should also adapt to an operation mode similar to that of confocal endoscopes that use single fibers or fiber bundles as optical relays.[3–8] The microendoscope probe would serve as the optical head at the end of the fiber relay and with negatively prechirped pulses would yield reduced SPM compared with the last few centimeters of an optical fiber.

Our microendoscope probes are compound GRIN triplets (Figs. 1a and 1c) that we used in an optical layout similar to that of a laser-scanning multiphoton microscope[1] (Fig. 1b). The triplet comprises an objective lens, a relay lens, and a coupling lens. For collecting maximum fluorescence, the objective numerical aperture (NA) should be close to the upper limit set by GRIN fabrication constraints, about 0.5. Thus, the pitch length, p (axial length for two full oscillations in beam diameter[15]), of the GRIN substrate for the objective is relatively short, only 3.7–9.5 mm. Our probes use a cylindrical GRIN substrate with an approximate quadratic radial variation in refractive index, $n(r) = n_0(1 - g^2r^2/2)$. p is determined by the coefficient g, $p = 2\pi/g$. The pitch of the objective lens, the axial lens length (L) in units of p, is less than 1/4 and is found from the working distance: $\mathrm{WD} = [gn_0 \tan(2\pi L/p)]^{-1}$. A collimated beam entering the objective is focused in the sample a distance WD from the external face (Fig. 1c). This is a focal distance $[gn_0 \sin(gL)]^{-1}$ from the principal plane.

The relay lens has a lower NA, 0.084–0.11, and hence a longer pitch length (15–45 mm). Such length is needed for insertion of the probe into a deep sample; for many applications a 1/2-pitch relay suffices. GVD is not too troublesome, since the on-axis dispersion coefficient of our GRIN lenses is ~6300 $\mathrm{fs}^2/\mathrm{cm}$ (Ref. 16). This dispersion implies that in our current longest probe of 2.6 cm an unchirped pulse in the range 100–120 fs broadens 76–42%. For additional length, the relay may be an integral multiple of 1/2-pitch, and in some cases prechirping may be warranted. The coupling lens is 1/4-pitch and its 0.5 NA matches the 0.5 NA of the microscope objective that focuses the excitation beam to just above the external face of the coupling lens (Figs. 1b and 1c).

The GRIN triplet translates an image plane from just external to the coupling lens to the focal plane in the sample (Fig. 1c). Magnification is calculated and measured to be near 1, since the probe objective and coupling lens are usually both near 1/4-pitch in length. To scan the excitation beam laterally within the sample, one scans the beam waist in the focal plane just above the coupling lens (Figs. 1b and 1c). The scanning optics are proximal to the light source and so need not be miniaturized. In the design of Fig. 1c, our aim was not only to preserve optical resolution and coupling efficiency of the excitation beam but also to minimize aberrations. To design an endoscope of a given length, it helps to choose a relay GRIN substrate with a long pitch length, because aberrations accrue in lenses of multiple pitch.[17] This choice comes at the expense of field of view, which is approximately the endoscope diameter divided by the ratio of relay pitch length to objective pitch length.[18] Other compromises are possible. In some cases, one might even choose to use a single multiple-pitch GRIN lens. In almost all GRIN endoscopes, peak pulse intensities occur only at the one, or at most the few, internal foci within the relay (Fig. 1c). This minimizes SPM.

The severity of SPM can be estimated by use of the B integral[15]

$$B \equiv \frac{2\pi}{\lambda} \int n_{2I}(z) I(z) \mathrm{d}z ,$$

which integrates the intensity, $I(z)$, weighted by the optical Kerr coefficient, n_{2I}, for wavelength λ, over the entire axial length of the instrument. The pulse acquires no significant SPM if $B < 1$. For the problem of femtosecond pulse delivery, one may calculate useful upper bounds on B by neglecting GVD. The condition $B < 1$ for a pulse of peak intensity, I_{peak}, traveling a length, L, in SMF implies $L < L_{\mathrm{SPM}} \approx \lambda/(2\pi n_{2I} I_{\mathrm{peak}})$. For two-photon microscopes with SMF delivery,[9,10] 100-fs pulses at 800 nm of 1 nJ imply $L_{\mathrm{SPM}} \approx 1.3$ cm, with $n_{2I} \approx 3 \times 10^{-16}$ cm^2/W for glass.[12] By contrast, 100-fs pulses accumulate significant GVD over ~9 cm,[12] indicating that SPM dominates GVD until I_{peak} falls. A central aim of our endoscope design was to achieve a smaller B value.

We calculated B for a GRIN lens. A beam with initial waist w_0 will have radius

$$w = w_0[\cos^2(gz) + C^2 \sin^2(gz)]^{1/2}$$

after propagating distance z within the lens, where $C = (\lambda/\pi g w_0^2 n_0)$ (Ref. 19). Neglecting GVD, we find that the B-integral over a lens of 1/4-pitch, $\pi/2g$, for a pulse of duration τ is

$$B \approx \frac{4n_{2I}E}{g\tau\lambda w_0^2} \int_0^{\pi/2} \frac{1}{(C^2 - 1)\sin^2(z') + 1} \mathrm{d}z' = \frac{2\pi^2 E n_0 n_{2I}}{\tau\lambda^2} .$$

Evaluation for 100-fs pulses at 800 nm yields a conservative bound to ensure minimal SPM, $E < 67$ nJ. This bound implies that GRIN endoscopes will retain quadratic dependence of two-photon fluorescence well beyond the pulse energy range commonly used for imaging. We verified this up to $E = 1.6$ nJ (Fig. 2a), using a 500-μm-diameter endoscope to excite a fluorescein dye solution.

To study endoscope resolving power, we imaged subresolution 100-nm fluorescent beads, using 810-nm excitation. As an estimate of lateral resolution, we used the full width at half-maximum (FWHM) of single bead images in a plane through the axial center of the bead (Fig. 2b). Endoscopes with NAs of 0.46, 0.42, and 0.26 displayed lateral resolutions of 1.26 ± 0.1 μm, 1.84 ± 0.1 μm, and 2.86 ± 0.2 μm, respectively (Fig. 2b). These FWHM values are approximately 2–2.5 times larger than expected from the theoretical treatment of resolution in two-photon imaging.[2] Aberrations probably cause this discrepancy. In addition to spherical aberration, chromatic

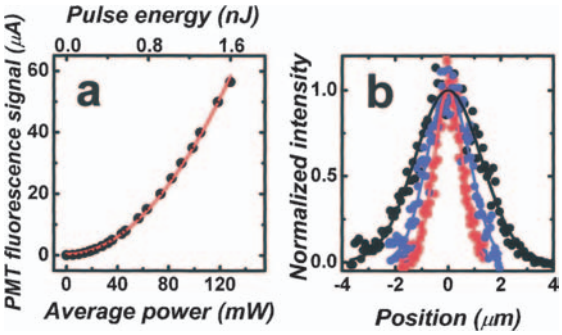

Fig. 2. a, Plot of the fluorescence signal generated by a fluorescein solution as a function of incident pulse energy and average power at 810 nm delivered by a 500-μm-diameter endoscope. Black circles, data; red curve, pure quadratic fit without a linear term, $y(x) = a + bx^2$. On a double-log plot, fluorescence rises with a slope of 1.96 ± 0.01. b, Line images of single 100-nm beads (Polysciences, Inc.), acquired in an axial plane through the bead center with 810-nm excitation. Intensity values are normalized to maximum intensity at the bead center. Red circles, data for a 1.0-mm-diameter endoscope with a 0.46 NA and 300-μm WD. Blue circles, data for a 500-μm-diameter endoscope with a 0.42 NA and a 300-μm WD. Black circles, data for a 500-μm-diameter endoscope with a 0.26 NA and an 800-μm WD. Solid curves, parametric fits. Fits to a Gaussian or to the square of the Airy disc (Ref. 2) are nearly indistinguishable, and both yield average FWHM of 1.26 ± 0.1 μm, 1.84 ± 0.1 μm, and 2.86 ± 0.2 μm.

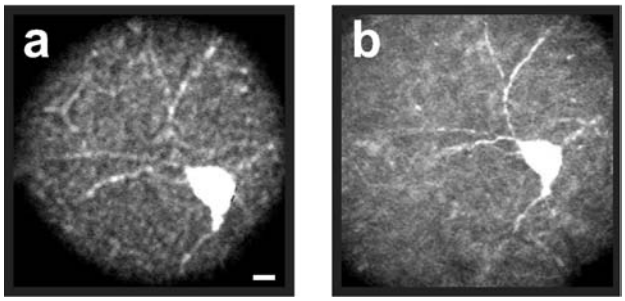

Fig. 3. Fluorescence images of a neuron and its dendrites in a zebra finch brain slice stained with Alexa-488 injected into brain area Hvc. Incident power at the sample was ~35 mW. A Nikon M-Plan 40× microscope objective with a 0.5 NA was used to match the 0.5 NA at the center of the endoscope's coupling lens. Angular and lateral misalignments lowered the optical transmission through the endoscope probe to ~55–65%. The 40× microscope objective magnification multiplies that of the endoscope probe. In a, the neuron was imaged with a 500-μm-diameter endoscope (0.54× magnification), with an endoscopic objective lens of 800-μm WD, 0.26 NA, and 122-μm field of view. The scale bar is 10 μm. In b, the identical neuron was imaged with a 1.0-mm-diameter endoscope (0.95×), with an endoscopic objective lens of 300-μm WD, 0.46 NA, and 211-μm field of view.

aberration may play a role: Some of our endoscopes exhibit a focal-length difference of ~1 μm or more across the ~12-nm spectral bandwidth of 800-nm excitation pulses.

We tested our ability to image cellular details by examining slices of zebra finch brain in which neurons were labeled with Alexa-488 fluorescent dye. After perfusion and fixation of the slices, we imaged neurons with a 500-μm-diameter endoscope with a 0.26-NA endoscopic objective (Fig. 3a; see caption for details) or with a 1.0-mm-diameter endoscope of 0.46 NA (Fig. 3b). Neuronal dendrites were visible, demonstrating the ability to resolve micrometer-scale subcellular features.

We introduced multiphoton fluorescence microendoscopes exhibiting micrometer-scale resolving power and minimal SPM. Our designs may also be useful for other forms of nonlinear optical imaging, such as those involving harmonic generation or coherent anti-Stokes Raman scattering. Given the widespread applicability of multiphoton microscopy, we anticipate that nonlinear optical endoscopy will rapidly be applied to live animal studies and eventually to human patient diagnostics.

We thank M. Fee and R. Hahnloser for the finch brain slices and R. Stepnoski and B. Messerschmidt for technical assistance. Bell Laboratories, McKnight Technological Innovations in Neuroscience, and the Human Frontiers in Science Program supported this work. Correspondence should be sent to schnitzer@lucent.com.

References

1. W. Denk and S. Svoboda, Neuron **18,** 351 (1997).
2. C. J. R. Sheppard and M. Gu, Optik (Stuttgart) **86,** 104 (1990).
3. D. L. Dickensheets and G. S. Kino, Opt. Lett. **21,** 764 (1996).
4. P. M. Lane, A. L. P. Dlugan, R. Richards-Kortum, and C. E. MacAulay, Opt. Lett. **25,** 1780 (2000).
5. A. R. Rouse and A. F. Gmitro, Opt. Lett. **25,** 1708 (2000).
6. R. Juskaitis, T. Wilson, and T. F. Watson, Scanning **19,** 15 (1997).
7. C. P. Lin and R. H. Webb, Opt. Lett. **25,** 954 (2000).
8. G. J. Tearney, M. Shishkov, and B. E. Bouma, Opt. Lett. **27,** 412 (2002).
9. D. Bird and M. Gu, Opt. Lett. **27,** 1031 (2002).
10. F. Helmchen, M. S. Fee, D. W. Tank, and W. Denk, Neuron **31,** 903 (2001).
11. D. G. Ouzounov, K. D. Moll, M. A. Foster, W. R. Zipfel, W. W. Webb, and A. L. Gaeta, Opt. Lett. **27,** 1315 (2002).
12. S. W. Clark, F. O. Ilday, and F. W. Wise, Opt. Lett. **26,** 1320 (2001).
13. F. Helmchen, D. W. Tank, and W. Denk, Appl. Opt. **41,** 2930 (2002).
14. M. T. Myaing, J. Urayama, A. Braun, and T. B. Norris, Opt. Express **7,** 210 (2000), http://www.opticsexpress.org.
15. A. E. Siegman, *Lasers* (University Science, Mill Valley, Calif., 1986).
16. B. Messerschmidt, T. Possner, and R. Goering, Appl. Opt. **34,** 7825 (1995).
17. D. C. Leiner and R. Prescott, Appl. Opt. **22,** 383 (1983).
18. J. Knittel, L. Schneider, G. Buess, B. Messerschmidt, and T. Possner, Opt. Commun. **188,** 267 (2001).
19. H. Kogelnik, Bell Syst. Tech. J. **44,** 455 (1965).